2.5

Autoconversion rate bias in stratiform boundary layer cloud parameterizations

R. WOOD *and P. R. FIELD *The Met Office, Bracknell, Berkshire, UK.*
W. R. COTTON *Department of Atmospheric Science, Colorado State University, Fort Collins, USA.*

Abstract

Because of their large grid-box size, global climate models do not explicitly represent small-scale processes occurring in cloud systems in the marine boundary layer. One such process, which is thought to have an important climatological effect is the production of warm rain. Parameterizations of this process typically partition the liquid water into a cloud and a rain component. The rate of conversion (autoconversion) of cloud to rain water is expressed as a convex function of the local cloud liquid water content. It is well known that the distribution of cloud liquid water content within boundary layer cloud systems is spatially non-uniform. This would result in biased mean autoconversion rates if no attempt is made to model subgrid variability. We examine three formulations, of increasing complexity, that can be used to model the distribution of liquid water content within a model grid-box and assess how well each predicts the mean autoconversion rate. Assuming complete homogeneity of cloud liquid water within a model grid-box results in large biases. The use of cloud fraction to partition the grid-box into cloudy and clear regions substantially reduces the biases. The most significant reduction of the biases is achieved with a Gaussian distribution of saturation excess within the grid-box. With this formulation, which could be facilitated using look-up tables, biases can be removed in a way consistent with the underlying distribution of saturation excess. We also present a simple parameterization that corrects much of the bias using simple algebraic expressions. It is demonstrated that to accurately calculate the mean autoconversion rate, an accurate parameterization of the width of the saturation excess distribution is required.

1. Introduction

Boundary layer cloud systems dominate the radiative balance in the subtropics (Slingo 1990). These systems typically extend over millions of square kilometres of ocean and have complex and self-similar structural properties (Lovejoy 1982; Cahalan and Snider 1989). The production of precipitation in marine boundary layer clouds in the subtropics is controlled almost exclusively by warm-rain microphysical processes (condensation, coalescence, sedimentation). Much work has beencarried out over the last three decades into the microphysics of warm rain (e.g. see Beard and Ochs 1993 for a brief review). In order to parameterize rainfall in large-scale numerical models many schemes partition the total condensed water into very small, essentially non-precipitating (cloud) droplets, and larger (rain) droplets which dominate the precipitation rate. Rain is produced in these schemes through an autoconversion process (cloud droplets collect each other to form rain drops) and an accretion process (rain drops falling through the cloud collect smaller cloud droplets). The autoconversion process is a local one, insofar as it depends upon local values of the droplet size distribution. It has been shown in a number of studies that the autoconversion rate is very strongly dependent upon the droplet size. For example, Khairoutdinov and Kogan (2000), henceforth KK, used a number of large-eddy simulations with explicit bin microphysics to show that the autoconversion rate is proportional to the droplet mean volume radius (r_{vol}) raised to the power of 5.67. Beheng (1994) also find a very high sensitivity of autoconversion upon droplet size. Therefore, for a given droplet concentration the autoconversion is strongly dependent upon the local cloud liquid water content. For the KK cases the autoconversion $A(q_C, N_d)$, when expressed as a function of local cloud liquid water content q_C and cloud droplet concentration N_d is fitted well using

$$A(q_C, N_d) = \left(\frac{\partial q_R}{\partial t}\right)_{auto} = K q_C^{\alpha} N_d^{\beta} \tag{1}$$

where K, α and β are constant (in the case of KK $\alpha = 2.47$, $\beta = -1.79$). Both Tripoli and Cotton (1980) and Beheng (1994) also present autoconversion formulations that take the form of Eqn. 1 with strong dependency of autoconversion rate upon local liquid water content ($\alpha = 7/3$ and $\alpha = 4.7$ respectively). The KK scheme is intended for use as a bulk microphysical parameterization in cloud resolving models but this does not necessarily preclude its use in larger scale models. The LES model from which the KK parameterization is derived has been validated against observations (Khairoutdinov and Kogan 1999) in stratocumulus cloud. The parameterization itself has been validated against observational data for a number of drizzling cases (Wood 2000) and is found to behave more favourably than the parameterizations of Kessler (1969), Tripoli and Cotton (1980) and Beheng (1994). We therefore consider the KK parameterization to be

*Current author address: Atmospheric Sciences, Box 351640, University of Washington, Seattle, WA, 98102, USA.

the most suitable bulk parameterization available for describing warm rain precipitation in large-scale numerical models.

Because these formulas refer to local values of the parameters involved, the question arises as to how to apply them for use in models with large grid-boxes, which have only either no representation or only a limited representation of subgrid variability. The application of Jensen's inequality to the problem (Larson et al. 2000) shows that if the grid-box mean value of liquid water content is used to derive the autoconversion, i.e. $A_{biased} = A(\overline{q_C}, N_d)$ then Eqn. 1 always results in an underprediction of the true (unbiased) grid-box mean autoconversion rate $A_{unbiased} = \overline{A(q_C, N_d)}$, providing $\alpha > 1$. This result assumes a constant droplet concentration within the grid-box such that autoconversion variations depend only upon cloud liquid water content variations. The resulting relative bias in the mean autoconversion rate has been termed the *grid box autoconversion bias*, *GACB*, and can be defined as

$$GACB = \frac{A_{unbiased} - A_{biased}}{A_{unbiased}} \tag{2}$$

where $A_{unbiased}$ is the true (unbiased) mean autoconversion rate, and A_{biased} is the modelled (biased) autoconversion rate, assuming only a limited representation of the subgrid variability. We refer to this bias as the relative grid-box autoconversion bias. It is also useful to represent the bias as the correction factor F that needs to be applied to the modelled bias A_{biased} to obtain the unbiased autoconversion rate:

$$F = \frac{A_{unbiased}}{A_{biased}} = \frac{1}{1 - GACB}. \tag{3}$$

For autoconversion rate formulations that, like Eqn. 1, depend upon the product of independent functions of q_C and N_d, the value of $GACB$ (and F) is independent of N_d, provided N_d is constant within the grid-box. This allows us to treat the autoconversion bias due to the subgrid variability in liquid water content without the need for measurements of droplet concentration. Of course, the absolute bias in the autoconversion rate does depend upon N_d, but the relative bias $GACB$ (and therefore F) does not. We do not examine variability in N_d or the possible correlations between N_d and q_C in this study, but note that it would be an interesting avenue of study.

Pincus and Klein (2000), using hypothetical liquid water content subgrid distributions representative of those in the marine boundary layer, show that biases in processes that depend non-linearly upon liquid water content can be as large as a factor of two. Further, they suggest that the unphysical and undesirable process of tuning GCM parameters so that top-of-atmosphere radiation budgets are balanced, may be necessitated to an extent by the nonaccounting for such biases in GCMs.

It should be noted that many GCMs now include either a prognostic or diagnostic cloud fraction variable. The aim of this paper is, first, to describe three different model formulations to describe liquid water content spatial variability within a large-scale model grid box, each with increasing complexity. We then proceed to quantitatively examine the magnitude of the autoconversion biases using observational data taken in stratiform marine boundary layer clouds. We pay particular attention to the scale-dependent nature of these biases. We quantitatively assess how increasing the complexity of the subgrid variability reduces the biases and also suggest a simple parameterization that can successfully remove much of the bias while avoiding the computationally expensive use of hypergeometric functions or look-up tables that are required in the Gaussian formulation.

2. Model formulations for subgrid variability and autoconversion biases

In this study we consider three frameworks that can be used to describe the distribution of liquid water content within a model grid-box. In inreasing order of complexity, these are: (a) Homogeneous: the available liquid water content is distributed uniformly through the entire grid-box; (b) the grid box is partitioned into cloud and clear air fractions using a cloud fraction and liquid water content is uniform within the cloudy fraction; (c) subgrid variability in liquid water content is described using a Gaussian distribution of saturation excess. Each of these distributions of liquid water content give different autoconversion rates. We examine this in detail below. Functions $GACB$ and F corresponding to each of the frameworks will be subscripted accordingly.

a. Homogeneous model

The homogeneous model is the simplest approach for modelling autoconversion and assumes that the liquid water content is distributed uniformly throughout the entire grid-box. Combination of Eqns. 1 and 2, gives the relative grid-box autoconversion bias of this homogeneous model:

$$GACB_{hom} = \frac{\overline{A(q_C, N_d)} - A(\overline{q_C}, N_d)}{\overline{A(q_C, N_d)}} = 1 - \frac{(\overline{q_C})^\alpha}{\overline{q_C^\alpha}}. \tag{4}$$

b. Black-white model

This approach to representing the subgrid variability assumes that both the mean liquid water content and cloud fraction are known. Then the distribution of cloud within a grid-box is treated as regions of clear air and regions of cloudy air with constant liquid water content. Thus, there is no cloud internal inhomogeneity. We call this a black-white model (after Mandelbrot 1983). The total area of cloud in the grid-box is the cloud fraction, C. The in-cloud liquid water content q_{cloud} is given by

$$q_{cloud} = \frac{\overline{q_C}}{C}. \tag{5}$$

where $\overline{q_C}$ is the grid-box mean liquid water content. This is predicted prognostically or diagnostically in large scale numerical models using a variety of cloud schemes (e.g. Smith 1990, Tiedtke 1993, Rotstayn 1997). The autoconversion bias $GACB_{BW}$ for the black-white model can be calculated using Eqns. 1, 2, and 5:

$$GACB_{BW} = 1 - \frac{(\overline{q_C})^\alpha}{C^{\alpha-1}\overline{q_C^\alpha}} \tag{6}$$

The black-white autoconversion bias is related to the homgeneous bias (combining Eqns. 4 and 6), so that the correction factors for the black-white and homogeneous formulations are related by $F_{BW} = C^{\alpha-1}F_{hom}$.

c. Gaussian distribution of saturation excess

The Gaussian framework describes subgrid variability of liquid water content completely using the assumption that the saturation excess is distributed using a Gaussian distribution. Large eddy simulations from a number of cloud regimes (Cuijpers and Bechtold 1995), from well-mixed stratocumulus-topped to trade-wind cumulus boundary layers, suggest that both cloud fraction C and grid-box mean liquid water content are well modelled as a single function of the normalised saturation excess Q_1:

$$Q_1 = \frac{a\left(\overline{q_t} - q_{sat}(\overline{T_l})\right)}{\sigma_s} \tag{7}$$

where $\overline{q_t}$ is the grid-box mean total water content and q_{sat} is the saturation specific humidity. Variables in Eqn. 7 are defined as

$$T_l = T - L_e q_C / c_p \tag{8}$$

$$s = a q_t' - b\theta_l' + c \tag{9}$$

$$a = \left\{1 + \frac{L_e}{c_p}\left(\frac{\partial q_{sat}}{\partial T}\right)_{T=T_l}\right\}^{-1} \tag{10}$$

$$b = a\frac{\overline{T}}{\overline{\theta}}\left(\frac{\partial q_{sat}}{\partial T}\right)_{T=T_l} \tag{11}$$

$$c = a\left(\overline{q_t} - q_{sat}(\overline{T_L})\right) \tag{12}$$

where L_e is the specific heat of vapourisation of water, q_C is the liquid water content, c_p is the specific heat capacity of air at constant pressure, T is the temperature, and θ_l is the liquid water potential temperature $\theta_l = \theta(1 - L_e q_C/c_p)$. Primes indicate deviations from the mean of that quantity. The probability distribution of s is given by

$$P(s) = \frac{1}{\sigma_s\sqrt{2\pi}}\exp\left\{-\frac{(s-\overline{s})^2}{2\sigma_s^2}\right\} \tag{13}$$

The Gaussian model is validated using aircraft observations in Section 3. Bougeault (1981) shows that for a Gaussian distribution of s, it is possible to write

$$C = \frac{1}{2}\left\{1 + \mathrm{erf}(Q_1/\sqrt{2})\right\} \tag{14}$$

$$\frac{\overline{q_C}}{\sigma_s} = CQ_1 + \frac{\exp(-Q_1^2/2)}{\sqrt{2\pi}} \tag{15}$$

where erf is the error function. Defining $I(a,z)$ as the a^{th} Gaussian partial moment integral given by

$$I(a,z) = \int_{x=z}^{x=\infty} (x-z)^a \exp\left(-\frac{x^2}{2}\right) dx, \tag{16}$$

the analytical form for $I(a,z)$ can be written as

$$I(a,z) = 2^{(a-1)/2}\exp\left(-\frac{z^2}{2}\right)\left[-\sqrt{2}z\Gamma\left(1+a/2\right)M\left(1+\frac{a}{2},\frac{3}{2},\frac{z^2}{2}\right)+\Gamma\left([1+a]/2\right)M\left(\frac{1+a}{2},\frac{1}{2},\frac{z^2}{2}\right)\right] \tag{17}$$

with $M(a,b,z)$ being the *1F1*-hypergeometric function (Abramowitz and Stegun 1970)

$$M(a,b,z) = 1 + \frac{az}{b} + \frac{a(a+1)z^2}{b(b+1)2!} + ... + \frac{a(a+1)..(a+n-1)z^n}{b(b+1)...(b+n+1)n!} + ... \tag{18}$$

Some mathematical manipulation using hypergeometric functions makes it possible to write down an analytical form for the Gaussian mean autoconversion rate:

$$\overline{A}_{Gauss} = KN_d^{\beta}\overline{q_C^{\alpha}} = KN_d^{\beta}\frac{\sigma_s^{\alpha}}{\sqrt{2\pi}}I(\alpha,-Q_1) \tag{19}$$

and therefore the autoconversion bias:

$$GACB_{Gauss} = 1 - \frac{\sigma_s^{\alpha}I(\alpha,-Q_1)}{\sqrt{2\pi}\,\overline{q_C^{\alpha}}}. \tag{20}$$

For a given value of α, the ratio of the Gaussian and homogeneous (or black-white) correction factors is a function only of the normalised saturation excess. This can be seen by combining Eqns. 4, 20, and 15 to give

$$F_{Gauss} = F_{hom}\frac{\sqrt{2\pi}}{I(\alpha,-Q_1)}\left(\frac{\overline{q_c}}{\sigma_s}\right)^{\alpha} = F_{hom}\frac{\sqrt{2\pi}}{I(\alpha,-Q_1)}\left\{CQ_1 + \frac{\exp(-Q_1^2/2)}{\sqrt{2\pi}}\right\}^{\alpha} \tag{21}$$

In the next section we turn to observational datasets to determine the potential magnitude of the homogeneous biases. Through the relationships between F_{hom}, F_{BW}, and F_{Gauss}, we then generalise our findings to ascertain the ability of the more complex black-white and Gaussian models to remove the biases.

3. Observations

Aircraft data used in this study are all taken from the *Met. Office* C-130 research aircraft which flew a total of 21 flights during the First ISCCP Regional Experiment (FIRE, 8 flights; Albrecht et al., 1988) and The Atlantic Stratocumulus Transition Experiment (ASTEX, 13 flights; Albrecht et al., 1995). Details of the thermodynamic instrumentation on the C-130 can be found in Rogers et al. (1995). Microphysical instrumentation is described in Martin et al. (1994). All data presented here are taken from constant-altitude runs in the boundary layer. Cloud fraction is calculated using the method described in Wood and Field (2000).

a. Cloud fraction/saturation excess/liquid water content relationships

We first validate the LES results of Cuijpers and Bechtold (1995) using aircraft data from FIRE and ASTEX. Figure 1 shows the cloud fraction as a function of the Q_1 for stratocumulus topped boundary layers. The data presented are taken from the FIRE and ASTEX flights reported in Wood and Field (2000). Most runs are between 50 and 70 km in length. Overplotted are the parameterizations of Cuijpers and Bechtold and the curve obtained assuming a Gaussian distribution of s. Note that both parameterizations agree fairly well with the observations. It is therefore concluded that, using the Gaussian distribution of saturation excess, the cloud fraction can be obtained to reasonable accuracy given grid-box mean temperature and total water content, provided the standard deviation of the function s is known. We find that σ_s is, in the mean, larger by almost a factor of two for ASTEX data than for FIRE data. We also find that σ_s scales with horizontal scale. To examine this we subdivide the aircraft runs into smaller sections (with lengths equal to 1/2, 1/4, 1/8 ... of the original run length) and calculate σ_s for these sub-sections. We then bin the data according to run length and calculate the mean value of σ_s for the dataset. Figure 1(b) shows the dataset mean values of σ_s as a function of run length L. Error bars represent the standard error in the mean at 95% confidence. Both FIRE and ASTEX exhibit almost identical power law scaling, which can be written

$$\langle\sigma_s\rangle = \alpha_s L^{\beta_s} \tag{22}$$

The fitted values for the exponent β_s are 0.32 $\pm$0.02 (FIRE) and 0.33 $\pm$0.02 (ASTEX). The values of α_s are 0.028 ± 0.001 and 0.050 ± 0.002 for FIRE and ASTEX respectively.

The expected value of the exponent β_s for a variable exhibiting Kolmogorov ("-5/3") power scaling is 1/3. The observationally-derived exponents are close to 1/3, suggesting that s follows Kolmogorov-like type of scaling across scales from hundreds of metres to tens of kilometres. The ratio of the standard deviation in ASTEX to that in FIRE is approximately 1.5-1.8 at all scales. The increased power in ASTEX compared to FIRE is a general finding supported by earlier observations (Davis et al. 1996). While the precise causes are not yet entirely clear, there is some support (Wood and Taylor 2001) for a positive correlation between boundary layer depth and the variance of temperature and humidity in the subtropical marine boundary layer. The boundary layer during ASTEX was significantly deeper than that during FIRE. Decoupling of the boundary layer is found more often in deeper boundary layers and this decoupling is likely to be associated with the generation of mesoscale cellular features and an upscale turbulent cascade. This may result in enhanced variance of the saturation excess at all scales. Large eddy simulations (LES) of a large-domain dry convective boundary layer (Jonker et al. 1999) found that passive scalars can spontaneously develop variability on horizontal scales significantly larger than the boundary layer depth. It is also possible that microphysical aspects themselves could play a role in the development of the enhanced mesoscale variability through evaporative cooling/moistening of the subcloud layer. Recent LES (Stevens et al. 2002) of a 20$\times$20 km cloudy domain show, however, that mesoscale circulations can develop in a cloudy trade-wind boundary layer without precipitation. An increase in computational power of the turbulence-resolving simulations, coupled with improved observations (especially those able to sample large areas such as satellites and radar), will give the opportunity of being able to focus on the mechanisms for mesoscale variability (Rossow et al. 2002).

Figure 1(c) shows observed liquid water content normalised with σ_s plotted against the normalised saturation excess Q_1. The dashed line represents the relationship obtained from the assumption of Gaussian s. The observed liquid water contents are smaller than the Gaussian ones for Q_1 larger than around 0. The Gaussian model appears to underestimate the liquid water contents at the smallest Q_1. However, observational errors in $\overline{q_C}$ are typically larger when this parameter is small, and so the divergence from the Gaussian model may be an artifact.

From Eqns. 14 and 15 it is clear that it is possible to express the cloud fraction solely as a function of the ratio $\overline{q_C}/\sigma_s$. This relationship is shown (solid line) in Fig. 1(d) together with observations from FIRE (circles) and ASTEX (triangles). The analytic form for the relationship between cloud fraction and normalised liquid water content $\overline{q_C}/\sigma_s$, formed by the combination of Eqns. 14 and 15, is complex and involves unwieldy hypergeometric functions. However, it is well parameterized using the exponential form

$$C = 1 - \exp\left(-1.9\frac{\overline{q_C}}{\sigma_s}\right) \tag{23}$$

which is given in Fig. 1(d) by the dashed line.

b. $GACB_{hom}$

Equations 4, 6 and 20 define the relative autoconversion biases for the three model formulations described in the previous section. We begin by examination of the magnitude of the biases that the homogeneous model and then examine how well the black-white and Gaussian models can reduce these biases.

To estimate $GACB_{hom}$ for a particular value of α we use Eqn. 4. To ascertain the scale-dependency of $GACB_{hom}$ we subdivide the aircraft runs into sub-runs with lengths of 1, 5, 10, 20, 30 and 60 km. All data used were taken at 4 Hz using a Johnson-Williams (J-W) liquid water content sensor. The details of the sensor are found in Rogers et al. (1995). The J-W probe has been shown (e.g. Davis et al. 1996) to have a reduced response to rapid changes in liquid water content at scales smaller than around 500 m (>0.2 Hz). At the aircraft speed of 100 m s^{-1} the 4 Hz sample rate gives 40 measurements for each kilometre of aircraft track. A $GACB_{hom}$ value is calculated for each sub-run and so for a single 60 km run, the number of subruns will be 2 (30 km), 3 (20 km), 6 (10 km), 12 (5 km) and 60 (1 km) subruns. We only expect the 1 km subruns to be affected by the response time limitations of the J-W probe. The total number of 60 km (or greater) runs used is 103 (FIRE) and 198 (ASTEX). Figure 2 shows an example of $GACB_{hom}$ values, calculated for the KK scheme ($\alpha = 2.47$), as a function of the run-mean liquid water content q_C. Here, data from all 30 km ASTEX sub-runs are shown. The $GACB_{hom}$ values here therefore represent the autoconversion bias that would result in a model with no representation of subgrid variability if we assume that the KK scheme has the correct dependency upon local liquid water content. The observed autoconversion bias is largest when the run-mean liquid water content is small and decreases as the liquid water content increases. The reason for this is that with small run-mean liquid water contents, the cloud fraction is generally smaller: the homogeneous model is less representative of reality at small cloud fractions.

We find that the observational $GACB_{hom}$-$\overline{q_C}$ data for each sub-run length L are fitted well using an exponential relation of the form

$$GACB_{hom} = \exp\left(-\frac{\overline{q_C}}{G(L)}\right) \tag{24}$$

where $G(L)$ is a function of the run length. To calculate the best-fit value of G we minimised *chi*-squared for the difference between the observed $GACB$ and that in Eqn. 24. This also allowed us to calculate errors in the best-fit values of G. Currently used parameterizations adopt values for α ranging from unity (e.g. Kessler 1969, if threshold is set to zero) to 4.7 (Beheng 1994). We choose a range of values of α to encompass the range of likely dependencies. The resulting best-fit values of G (for values of α=1.5, 2.0, 2.5, 3.0, 4.0, 5.0) are shown in Fig. 3 as a function of sub-run length L for the FIRE (3(a)) and ASTEX (3(b)) datasets. There are two important features:

(i) For a particular value of α, the function $G(L)$ is larger for ASTEX than for FIRE data;
(ii) The value of $G(L)$ increases with L for both FIRE and ASTEX datasets;

This indicates that for a particular run-mean liquid water content the biases are greater for ASTEX cloud systems than for FIRE ones, and is a result of there being generally greater variability in the liquid water contents in cloud systems typical of ASTEX boundary layers (Davis et al. 1996) caused by greater variability in the saturation excess (Fig. 1b). We should also note that removing the 1 km subruns from the analysis did not result in a significant difference in the fits, which suggests that the response time limitations of the J-W probe have little impact upon our results. The relationship can be represented using a power law of the form

$$G = \alpha_G L^{\beta_G} \tag{25}$$

where α_G and β_G are constants for each dataset and exponent α. Values of α_G, derived from the observations using chi-squared fitting, are shown in Fig. 4 for the FIRE and ASTEX datasets. The relationship between α_G and α is approximately linear for each dataset. The higher α_G values for ASTEX are indicative of greater variability at all scales. Whilst the values of α_G are clearly different for the ASTEX and FIRE observations, the power exponents β_G are not significantly different at the 95% level (0.32$\pm$0.03 for FIRE; 0.29$\pm$0.02 for ASTEX). We found no systematic variation of β_G with α for $2 < \alpha < 5$. It is not known why the data for $\alpha = 1.5$ differ from those at higher α, although it is noted that the exponential form (Eqn. 24) does not provide as good a fit to the data as α approaches unity.

4. Bias as a function of cloud fraction

a. C<1

Equation 24 describes how the grid-box autoconversion bias changes with run-mean liquid water content.

Given that the exponential form Eqn. 23 represents a reasonable model for the relationship between mean liquid water content and cloud fraction, we proceed by rearranging Eqn. 23 and substituting $\overline{q_C}$ in Eqn. 24 to give a parameterized bias, viz.

$$GACB_{hom,param} = (1 - C)^{\sigma_s(L)/1.9G(L)} \qquad (C < 1). \tag{26}$$

Thus $GACB_{hom,param}$ is a function of cloud fraction C and the potentially scale-dependent function $\sigma_s(L)/G(L)$. Figure 5 shows the values of G plotted against σ_s for three values of α=2.0 (triangles), 3.0 (circles), 5.0 (squares) for FIRE (filled symbols) and ASTEX (open symbols). It is clear that G is well parameterized as a function of σ_s. For each value of α a single relationship exists between σ_s and G for FIRE and ASTEX. It is therefore concluded that the difference in α_G values between FIRE and ASTEX is a result of differences in variability between the two datasets. Because there is, in general, more variability in ASTEX boundary layers, the values of G (and therefore $GACB$) are generally larger. The three lines are linear fits to the data for each value of α, which may be represented by

$$G(L) = f(\alpha)\sigma_s \tag{27}$$

with $f(\alpha)$ a linear function of α as shown in the inset of Fig. 5, which is found to be given by $f(\alpha) = 1.15(\pm 0.16)(\alpha - 1)$. Estimated errors are given at the 2-σ level.

The data suggest that it is possible to effectively correct the autoconversion bias if the variance in the boundary layer thermodynamic variable s can be obtained. The boundary layer cloud schemes of Bechtold (1995), Cuijpers and Bechtold (1995) and Lenderink and Siebesma (2000) propose parameterizations of the variance in thermodynamic parameters for use in large scale numerical models. In these schemes the variance is diagnosed as a function of vertical gradients in mean thermodynamic quantities (specific humidity and potential temperature) and turbulence length or velocity scales. This work is a substantial improvement on schemes such as Smith (1990) whose distribution width is a fixed function of temperature and pressure and a critical relative humidity parameter which is typically a fixed function of height. An improvement to this scheme has been proposed by Cusack et al. (1999) who attempts to predict subgrid variability from resolved information at larger scales. However, in boundary layer clouds, a considerable amount of the variance on the

mesoscale may be the result of turbulence upscaling and other nonlinear processes (e.g. Shao and Randall 1996). These processes have yet to be considered in parameterizations for large-scale numerical models.

Substituting equation 27 into 26 gives

$$GACB_{hom,param} = (1-C)^{1/(2.2(\alpha-1))} \tag{28}$$

which leads to a parameterization of the relative autoconversion bias as a function only of cloud fraction. For the Khairoutdinov and Kogan (2000) scheme (α=2.47), we obtain the relationship $GACB_{hom,param} = (1-C)^{0.31\pm0.04}$.

As an alternative to proceeding to Eqn. 28 via the exponential relationship Eqn. 24, we can use the FIRE and ASTEX data to find the best fit between C and $GACB_{hom}$

$$GACB_{hom,param} = (1-C)^{\gamma}\,. \tag{29}$$

We use *chi*-squared fitting of $GACB_{hom}$ vs C data to find the values of the exponent γ from the FIRE and ASTEX observations for different sub-run lengths L and find remarkably little dependence of γ upon L, as expected from Eqn. 28. The mean values of γ calculated for the six lengthscales are 0.34$\pm$0.02 (FIRE) and 0.35$\pm$0.02 (ASTEX), which are only slightly higher than the value predicted using Eqn. 28 and within the margin of error. We therefore conclude that, not only is there little or no scale dependence in the parameterization of $GACB$ as a function of cloud fraction, the same constant γ (approximately 0.34-0.35) is suitable for both FIRE and ASTEX. We carried out the same analysis for different values of α and found that the relationship Eqn. 28 fitted the observed data well.

The median observationally derived values of the correction factors ($\alpha = 2.47$) that would need to be applied to the model autoconversion rates to give the observed rates, are plotted as a function of cloud fraction in Fig. 6, for the three model formulations. Values close to unity indicate that the model corrects the biases well. The parameterization based upon Eqn. 29 with γ=0.31 is also shown. An important point is that the data from FIRE and ASTEX collapse onto almost the same curves. The homogeneous model autoconversion rates are incorrect by a factor of two or greater when $C < 0.8$. The black-white model (assuming the cloud fraction can be correctly predicted) reduces the biases compared with the homogeneous model but does not completely remove them. Both the Gaussian model and the parameterization reduce the biases to less than 30% for $C > 0.2$. For other values of $\alpha > 1$, the curves are qualitatively similar. The problem of parameterizing the bias at $C = 1$ is explored in section 3.2.

b. C=1

The $GACB_{hom}$ parameterization Eqn. 29, gives $GACB_{hom} = 0$ (i.e. $F_{hom} = 1$) when $C = 1$, which is clearly a shortcoming. It would be sensible not to use Eqn. 29 when the cloud fraction is approaching unity. We extracted all the observational data with $C > 0.95$ from the datasets and find that $GACB_{hom}$ in these cases scales well with $\overline{q_C}/\sigma_s$, i.e. the ratio of the mean liquid water content to the standard deviation of saturation excess. This is what we would expect from Eqn. 24 and the result that the values of G are linearly related to σ_s (Fig. 5). We plot the correction factors F for the different formulations against $\overline{q_C}/\sigma_s$ in Fig. 7. In these cases, $\alpha = 2.47$, although qualitatively similar results are obtained for different exponents. For fully cloudy runs, $F_{BW} = F_{hom}$. It is clear that the biases for the homogeneous/black-white formulations are considerably lower than those for the broken cloud runs. However, there remains a considerable under-prediction of the autoconversion rates which is quite well corrected using the Gaussian formulation or the parameterization Eqn. 24. The parameterized autoconversion rates use Eqn. 24 with G from observed σ_s and Eqn. 27 (with respective constants α_G for FIRE and ASTEX).

c. Summary of suggested parameterization for $GACB$

We propose a method to correct the bias in autoconversion rate in large-scale numerical models incurred by poor or no treatment of the subgrid variability in liquid water content. In this study, we assume that locally, the autoconversion rate is proportional to the liquid water content to some power α as in Eqn. 1 and that the droplet concentration is constant within the grid-box. Insofaras this model is realistic, the autoconversion bias for a model with a homogeneous formulation of liquid water content can be formulated either in terms of mean liquid water or cloud fraction:

$$GACB_{hom} = \begin{cases} (1-C)^{1.0/(2.2(\alpha-1))} & (C < 1 \text{ only}) \\ \exp\left(-\overline{q_C}/G(L)\right) & (C = 1) \end{cases} \tag{30}$$

$$\text{where } G(L) = 1.15(\alpha-1)\sigma_s \tag{31}$$

with σ_s being a scale dependent function which itself requires parameterization. We do not address the issue of parameterizing σ_s here. The correction factor $F_{hom} = 1/(1-GACB_{hom})$ can then be calculated and applied to the biased autoconversion rate to remove the bias.

For numerical models that predict cloud fraction and then use the in-cloud liquid water content q_{cloud} calculated using Eqn. 5 to derive the mean autoconversion rate (black-white formulations), the correction factor $F_{BW} = C^{\alpha-1}F_{hom}$ would be applied to the black-white grid-box mean autoconversion rate. Autoconverision rates calculated using the integral over the full Gaussian pdf of saturation excess do not require significant additional correction because the biases are quite effectively removed with this technique. However, the Gaussian autoconversion rate calculation involves a numerical evaluation of the *1F1*-hypergeometric function (Eqn. 19). We find that third-order polynomial fits to the logarithm of $I(\alpha, -Q_1)$ can be used to generate a simple interpolating look-up table that can be used to calculate the autoconversion rates for the Gaussian pdf with errors not exceeding 1% $(1.5 < \alpha < 4.5; Q_1 > -2)$.

Clearly the autoconversion bias parameterization for $C < 1$ does not depend upon the particular cloud regime (i.e. the same equation works for FIRE and ASTEX), but for $C = 1$ a regime-dependent form is required. However, it should be noted that the parameterization of cloud fraction is both scale- and regime-dependent (as demonstrated in section 3(a)). As stated earlier the differences in $G(L)$ between FIRE and ASTEX result from differences in σ_s between the two regimes. In addition, it is not clear how accurate the parameterization will be for non-boundary layer cloud systems. Rather than presenting a definitive and exhaustive parameterization of the autoconversion bias, this study is aimed (a) highlighting how the autoconversion bias is closely tied to the mean and standard deviation of the distribution of s, and (b) providing a dataset for possible testing of parameterizations of subgrid variability.

5. Discussion and conclusions

Biases in autoconversion rate can arise in large scale models when subgrid variability in liquid water content is ignored. The use of aircraft observations from a number of flights during two field programs has allowed us to estimate the magnitude of such biases. We find that the biases increase with increasing run length (equivalent to model grid-box size), and that for the same grid-box mean liquid water content and run length, the mean biases are greater during ASTEX than during FIRE. However, because ASTEX clouds require a higher mean liquid water content than FIRE clouds to achive the same cloud fraction (due to greater variability in ASTEX clouds), it is shown that the bias can be represented as a single function of cloud fraction which is independent of (a) the location (FIRE, ASTEX) and (b) the run length. It is suggested that this behaviour could be useful in attempting to correct the biases. However, because the variance of saturation excess is a scale dependent variable, the cloud fraction is also a scale dependent function of the mean saturation excess, and should be treated as such in large-scale numerical models. It is also shown how the use of cloud fraction to represent, at least in part, some of the subgridscale variability, removes quite effectively some of the bias. However, when the cloud fraction is unity, this approach can lead to significant biases in autoconversion rate.

The question of how to apply the results presented here to develop better representation of cloud variability is a pertinent one. The observations presented here provide a test-bed for estimates of the autoconversion bias using probability distribution functions to represent the subgrid variability. Future parameterizations which predict subgrid variability from large-scale forcings should be able reproduce the observed differences in grid-box autoconversion bias between the mid-Atlantic (ASTEX) stratocumulus region and the Californian (FIRE) region. Cusack et al. (1999) used model simulations using a relatively small grid-box size to parameterize subgrid variability at larger scales. They found that the spectral power between horizontal scales of 150 km and 400 km varied considerably with location. This novel approach could in future be built upon using nested models which span a wider range of scales from cloud resolving model to climate model grid-box sizes to achieve greater understanding of the physical causes for inhomogeneity. Detailed satellite measurements using a range of sensor resolutions and domain sizes spanning scales from metres to thousands of kilometres have shown that robust scaling relationships exist in nature. Understanding the physical basis for these relationships is a primary goal of future research.

In addition to variability in liquid water content, there is likely to be subgrid variability in droplet concentration due to mesoscale variability in updraught speed and CCN concentration. In this study we have considered that biases in autoconversion result only from heterogeneity in liquid water content. There are physical reasons why droplet concentration may be correlated with liquid water content (or liquid water path) that may result in quite complex biases in autoconversion. In future it also may be possible to represent droplet spectra within a gridbox using a moment scheme such as that presented in Feingold et al. (1998). With schemes such as this, the concepts of autoconversion and accretion are addressed in a more physically realistic manner than by simply partitioning into cloud and rain water. Nevertheless, for large gridbox sizes, neglect of subgrid variability will result in biases; parameterizing the subgrid variability will be a challenge.

References

Abramowitz M., and Stegun, I. (1970) Handbook of Mathematical Functions, Dover Publications Inc., New York.

Albrecht, B. A., Randall, D. A., and Nicholls, S. N. (1988) Observations of marine stratocumulus during FIRE. *Bull. Am. Meteorol. Soc.*, **69**, 618–626.

Albrecht, B. A., Bretherton, C. S., Johnson, D. W., Schubert, W. H., and Frisch, A. S. (1995) The atlantic stratocumulus transition experiment - ASTEX. *Bull. Am. Meteorol. Soc.*, **76**, 889–904.

Beard, K. V., and Ochs H. T., (1993) Warm-rain initiation: An overview of microphysical mechanisms. *J. Appl. Meteorol.*, **32**, 608–625.

Bechtold, P., Cuijpers, J. W. M., Mascart, P., and Trouilhet, P. (1995) Modelling of trade wind cumuli with a low-order turbulence model: toward a unified description of Cu and Sc clouds in meteorological models. *J. Atmos. Sci.*, **52**, 455–463.

Beheng, K. D., (1994) A parameterization of warm cloud microphysical processes. *Atmos. Res.*, **33**, 193–206.

Bougeault, P., (1981) Modeling the trade-wind cumulus boundary layer. Part I: testing the ensemble cloud relations against numerical data. *J. Atmos. Sci.*, **38**, 2414–2428.

Cahalan, R. F., and Snider, J. B., (1989) Marine stratocumulus structure. *Remote Sens. Environ.*, **28**, 95–107.

Cuijpers, J. W. M., and Bechtold, P. (1995) A simple parameterization of cloud water related variables for use in boundary layer models. *J. Atmos. Sci.*, **52**, 2486–2490.

Cusack, S., Edwards, J. M, and Kershaw, R., (1999) Estimating the subgrid variance of saturation, and its parametrization for use in a GCM cloud scheme. *Quart. J. Roy. Meteorol. Soc.*, **125**, 3057–3076.

Davis, A., Marshak, A., Wiscombe, W. J. and Cahahlan, R. F., (1996) Scale invariance of liquid water distributions in marine stratocumulus. Part 1: Spectral properties and stratonarity issues. *J. Atmos. Sci.*, **53**, 1538–1558.

Feingold, G., Walko, R. L., Stevens, B., and Cotton, W. R., (1998) Simulations of marine stratocumulus using a new microphysical parametrization scheme. *Atmos. Res.*, **47-48**, 505–528.

Jonker, H. J. J., Cuijpers, J. W. M. and Duynkerke, P. G., (1999) Mesoscale fluctuations in scalars generated through boundary layer convection. *J. Atmos. Sci.*, **56**, 801–808.

Kessler, E., (1969) On the distribution and continuity of water substance in atmospheric circulations. *Meteor. Monogr.*, **32**, Amer. Meteorol. Soc., 1-84.

Khairoutdinov, M. and Kogan, Y. L., (2000) A new cloud physics parametrization in a large-eddy simulation model of marine stratocumulus. *Mon. Wea. Rev.*, **128**, 229–243.

Khairoutdinov, M. and Kogan, Y. L., (1999) A large eddy simulation model with explicit microphysics: validation against aircraft observations of a stratocumulus-topped boundary layer. *J. Atmos. Sci.*, **56**, 2115–2131.

Larson, V. E., Wood, R., Field, P. R., Golaz, J.-C., Vonder Haar, T. H., and Cotton, W. R., (2000) Systematic biases in the microphysics and thermodynamics of numerical models that ignore subgrid-scale variability. Submitted to *J. Atmos. Sci.*, November 1999.

Lenderink, G., and Siebesma, A. P. (2000) Combining the massflux approach with a statistical cloud scheme. *Proceedings of the 14th Symposium on Boundary Layers and Turbulence*, Aspen, Colorado, USA, 7-11 August, 2000.

Lovejoy, S., (1982) Area-perimeter relation for rain and cloud areas. *Science*, **216**, 185-187.

Mandelbrot, B., (1983) *The Fractal Geometry of Nature.* W. H. Freeman, New York, 460pp.

Martin, G. M., Johnson, D. W., Rogers, D. P., Jonas, P. R., Minnis P., and Hegg, D. A. (1995) Observations of the interaction between cumulus clouds and warm stratocumulus in the marine boundary layer during ASTEX, *J. Atmos. Sci.*, **52**, 2902–2922.

Pincus, R., and Klein, S. A., (2000) Unresolved spatial variability and microphysical process rates in large

scale models. Submitted to *J. Geophys. Res.*, April 2000.

Rogers, D. P., Johnson, D. W., and Friehe, C. A. (1995) The stable internal boundary layer over a coastal sea. Part I: Airborne measurements of the mean and turbulence structure. *J. Atmos. Sci.*, **52**, 684–696.

Rossow, W. B., Delo, C., and Cairns B., (2002) Implications of the Observed Mesoscale Variations of Clouds For Earth's Radiation Budget. *J. Clim.*, in press.
Rotstayn, L. D., (1997) A physically based scheme for the treatment of stratiform clouds and precipitation in large scale models. *Quart. J. Roy. Meteorol. Soc.*, **123**, 1227–1282.

Slingo, A. (1990) Sensitivity of the earth's radiation budget to changes in low clouds. *Nature*, **343**, 49–51.

Shao, Q., and D. A. Randall. (1996) Closed Mesoscale Cellular Convection Driven by Cloud-Top Cooling. *J. Atmos. Sci.*, **53**, 2144-2165.

Smith, R. N. B. (1990) A scheme for predicting layer clouds and their water content in a general circulation model. *Quart. J. Roy. Meteorol. Soc.*, **116**, 435–460.

Stevens, D. E., Ackerman, A., and C. S. Bretherton. (2002) Effects of domain size and numerical resolution on the simulation of shallow cumulus convection. *J. Atmos. Sci.*, it submitted manuscript.

Tiedtke, M. (1993) Representation of clouds in large-scale models. *Mon. Wea. Rev.*, **121**, 3041-3061.

Tripoli, G. J. and Cotton, W. R., (1980) A numerical investigation of several factors contributing to the observed variable intensity of deep convection of south Florida. *J. Appl. Meteorol.*, **19**, 1037–1063.

Xu, K-M. and Randall, D. A. (1996) A semiempirical cloudiness parameterization for use in climate models. *J. Atmos. Sci.*, **53**, 3084–3102.

Wood, R., and Field, P. R. (2000) Relationships between total water, condensed water and cloud fraction examined using aircraft data. *J. Atmos. Sci.*, **57**, 1888–1905.

Wood, R. (2000) The validation of drizzle parametrizations using aircraft data. *Proceedings of the 13th International Conference on Clouds and Precipitation*, Reno, Nevada, USA, 14-18 August 2000.

Wood, R., and Taylor, J. P. (2001) Liquid water path variability in unbroken marine stratocumulus cloud. *Quart. J. Roy. Meteorol. Soc.*, **127**, 2635–2662.

Figure captions

Figure 1. (a) Cloud fraction from observations (all 60 km runs) plotted against normalised saturation excess Q_1 defined in Equation 7. Also shown are the proposed parameterization of Cuijpers and Bechtold (C+B 95, dotted line) based upon LES results, and the relationship obtained if a Gaussian distribution of s is assumed (dashed line). (b) Dataset mean values of σ_s as a function of run length L. The dotted and dashed lines are power law fits to the FIRE and ASTEX data respectively. The solid line shows the (1/3) power law expected if s follows a (-5/3) power spectral scaling. (c) Mean liquid water content normalised with σ_s plotted against Q_1 for FIRE and ASTEX data. (d) Cloud fraction against mean liquid water content normalised with σ_s. Dashed line shows Gaussian form which is well parameterized by a more simple exponential form (dashed line, Eqn. 23).

Figure 2. Example of relationship between $GACB_{hom}$ and run-mean liquid water content $\overline{q_C}$ for $\alpha = 2.47$. Observational data from runs of length 30 km from ASTEX is shown. It is clear that the autoconversion bias decreases with increasing run-mean liquid water content and is fitted reasonably well using a relation of the form $GACB_{hom}$ =exp$(-G\overline{q_C})$ (dashed line). The exponential is fitted by minimising *chi*-squared differences between the observed and parameterized $GACB_{hom}$.

Figure 3. Best fit grid box autoconversion bias parameter G as a function of sub-run length L and autoconversion exponent α for the FIRE (a, left) and ASTEX (b, right) datasets. Both FIRE and ASTEX data exhibit quite well-defined power law scaling - the dashed line has a power law scaling of $L^{1/3}$, apart from the data for $\alpha = 1.5$. It is uncertain why the power law scaling at $\alpha = 1.5$ is different.

Figure 4. Values of the prefactor α_G (Eqn. 24) against the autoconversion exponent α for FIRE (circles) and ASTEX (triangles) data. There is no bias (hence $\alpha_G = 0$) when the local liquid water content and autoconversion rate are linearly related ($\alpha = 1$). The dotted and dashed lines represent straight line fits to the data passing through point ($\alpha = 1$;$\alpha_G = 0$). The ratio of the gradients of the ASTEX and FIRE fits is approximately 1.6.

Figure 5. Plot of σ_s against G from FIRE (filled symbols) and ASTEX (open symbols). Data are only shown for α=2.0 (triangles), 3.0 (circles) and 5.0 (squares). Lines are linear fits to data for each value of α. The gradient of these fits $f(\alpha)$ is plotted as a function of α in the inset.

Figure 6. Median values of the multiplication correction factor F required to correct homogeneous (dash-dot), black-white (dot) and Gaussian (solid) formulations of autoconversion rate for broken clouds, plotted as a function of cloud fraction. Correction factors for the parameterization (Eqn. 30) are also shown (dashed). The Gaussian model and the parameterization both result in autoconversion rates that are within 30% of those derived using the observations for $C > 0.2$, whereas the black-white model tends to underpredict autoconversion rates by 30-100%.

Figure 7. Median values of the multiplication correction factor F for fully cloudy runs ($C > 0.95$), plotted against $\overline{q_C}/\sigma_s$. For $\overline{q_C}/\sigma_s > 2$, the Gaussian and parameterized (Eqn. 30) autoconversion rates are within 7% of the observationally derived ones. Both formulations appear to somewhat overcorrect at lower values of $\overline{q_C}/\sigma_s$. Note that the black-white and homogeneous formulations have the same biases when $C = 1$. However, there are only a very few cases during FIRE and ASTEX where $C > 0.95$ and $\overline{q_C}/\sigma_s < 2$, and so this may be a statistical artifact.

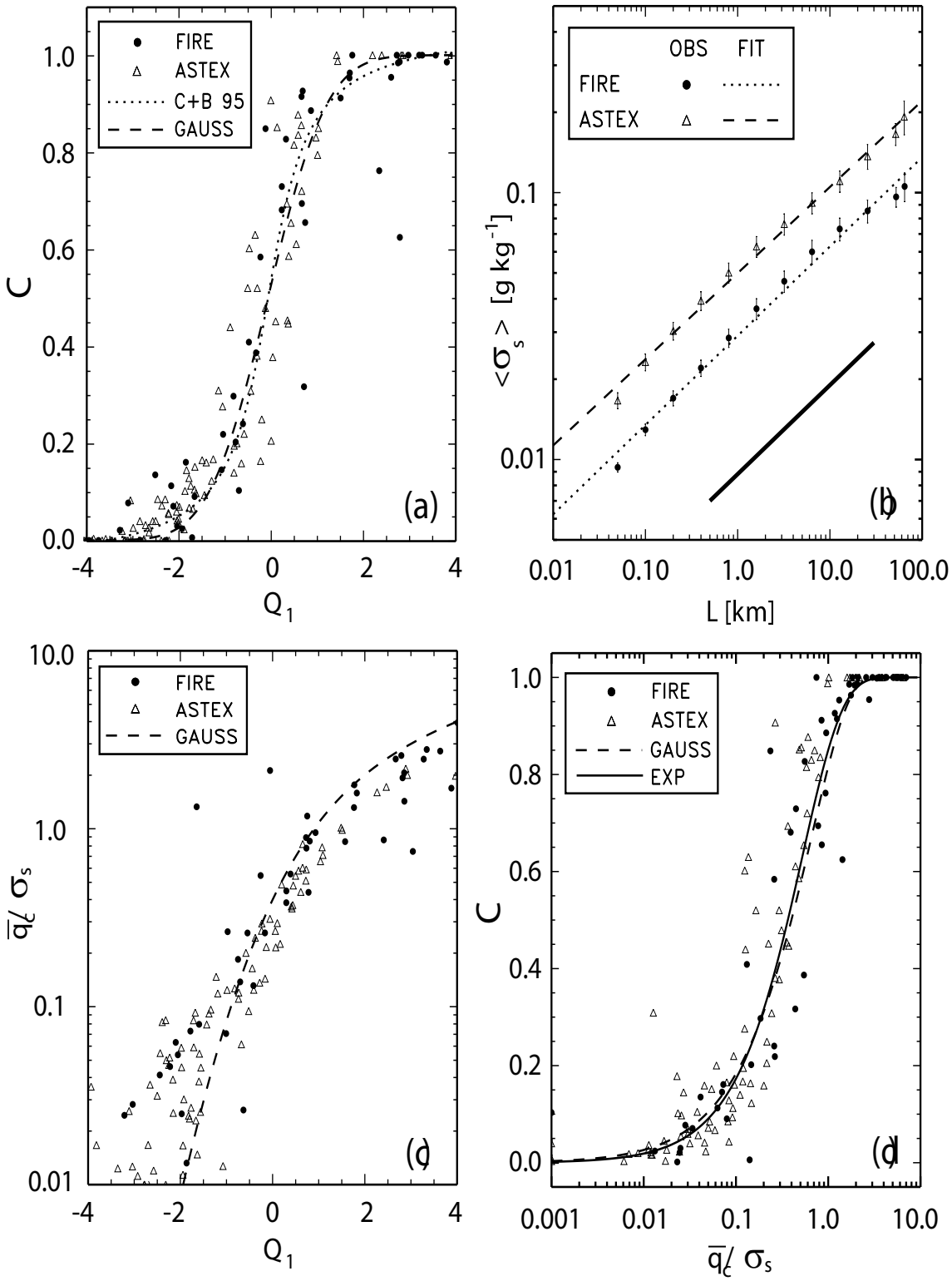
FIRE
ASTEX
C+B 95
GAUSS
C
Q_1
(a)
OBS FIT
FIRE
ASTEX
$<\sigma_s>$ [g kg^{-1}]
L [km]
(b)
FIRE
ASTEX
GAUSS
$\overline{q_\ell}/\ \sigma_s$
Q_1
(c)
FIRE
ASTEX
GAUSS
EXP
C
$\overline{q_\ell}/\ \sigma_s$
(d)

Figure 1:

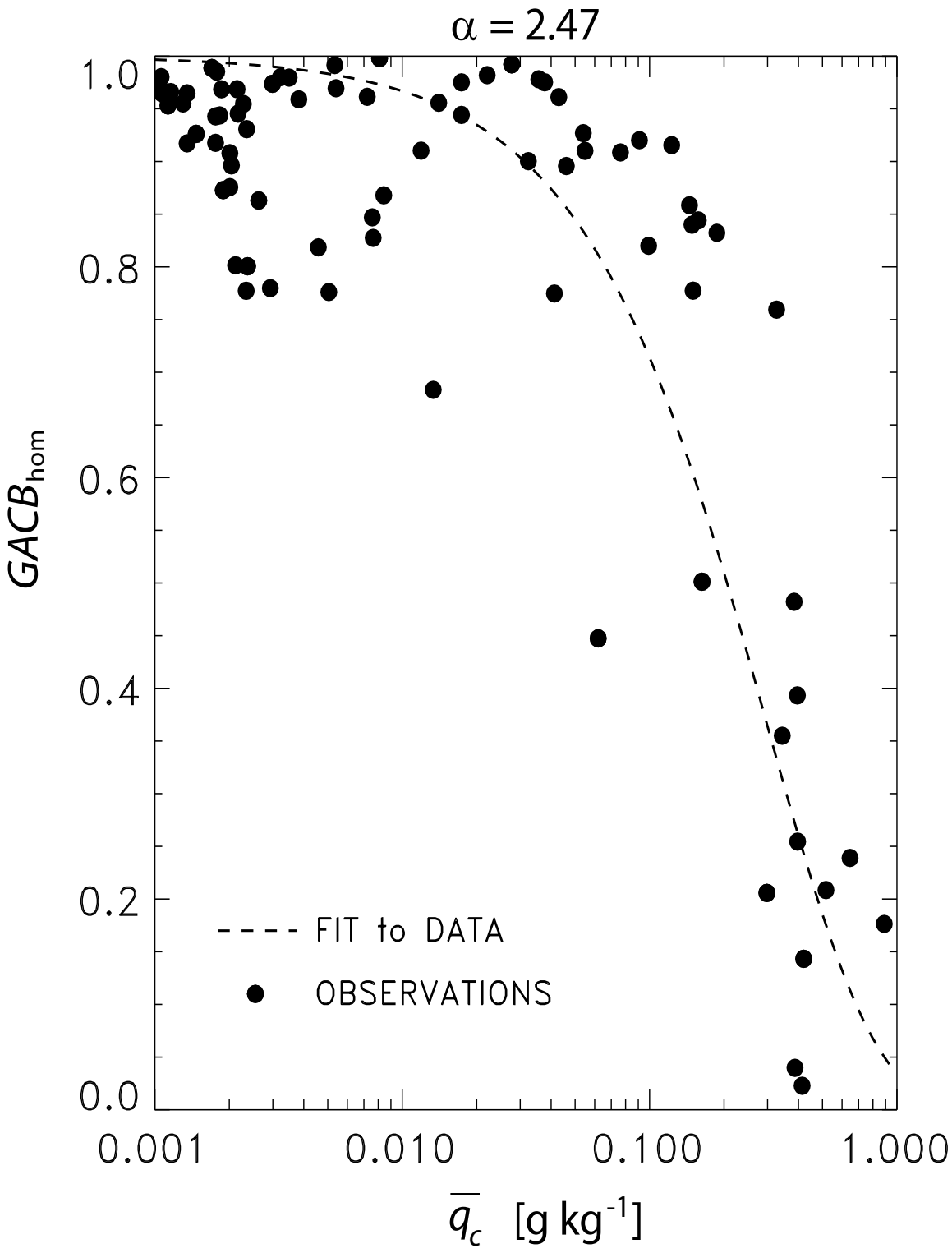
α = 2.47
1.0
0.8
0.6
0.4
0.2
0.0
GACB_hom
FIT to DATA
OBSERVATIONS
0.001
0.010
0.100
1.000
q_c [g kg^-1]

Figure 2:

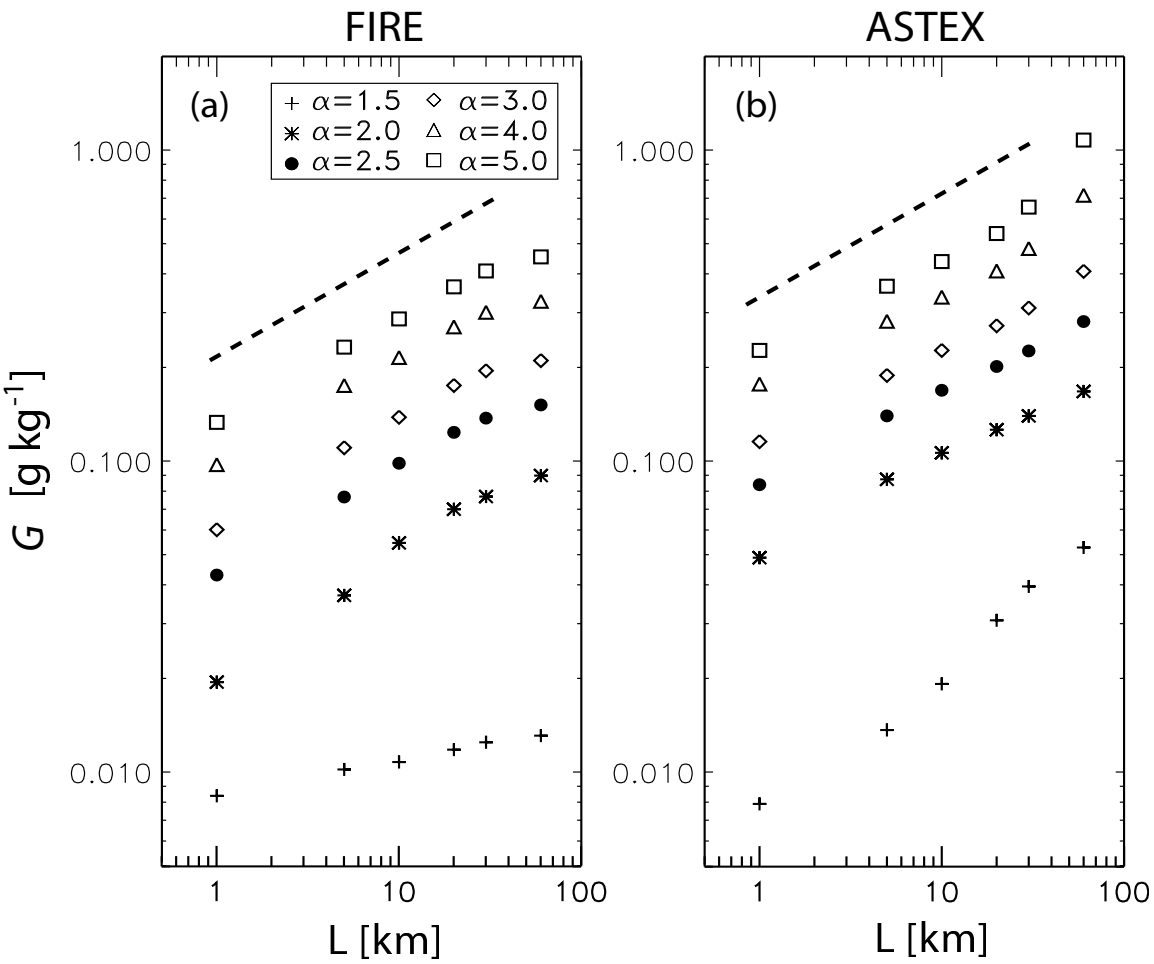
FIRE
ASTEX
(a)
(b)
α=1.5
α=2.0
α=2.5
α=3.0
α=4.0
α=5.0
1.000
0.100
0.010
G [g kg-1]
1
10
100
L [km]

Figure 3:

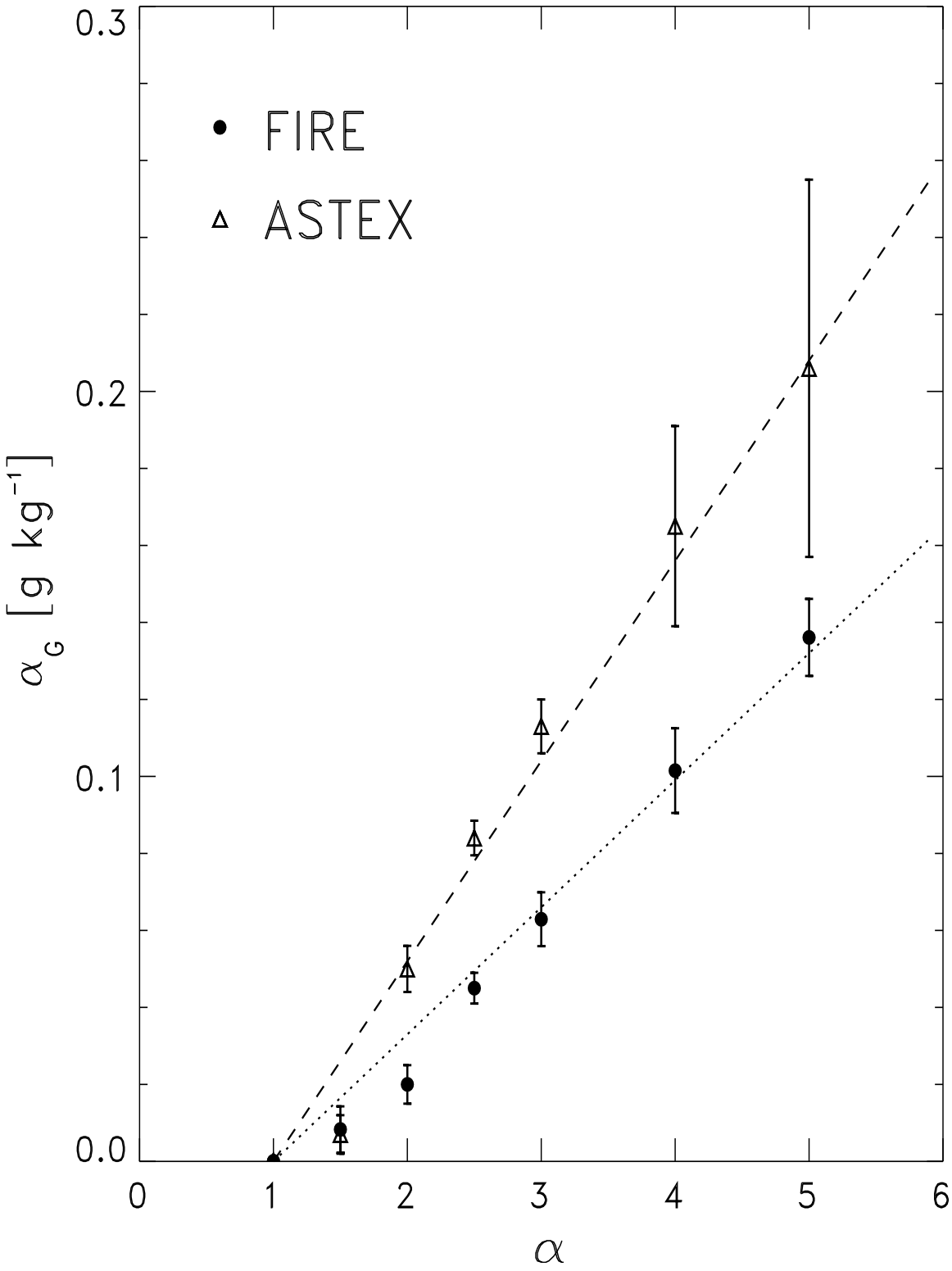

Figure 4:

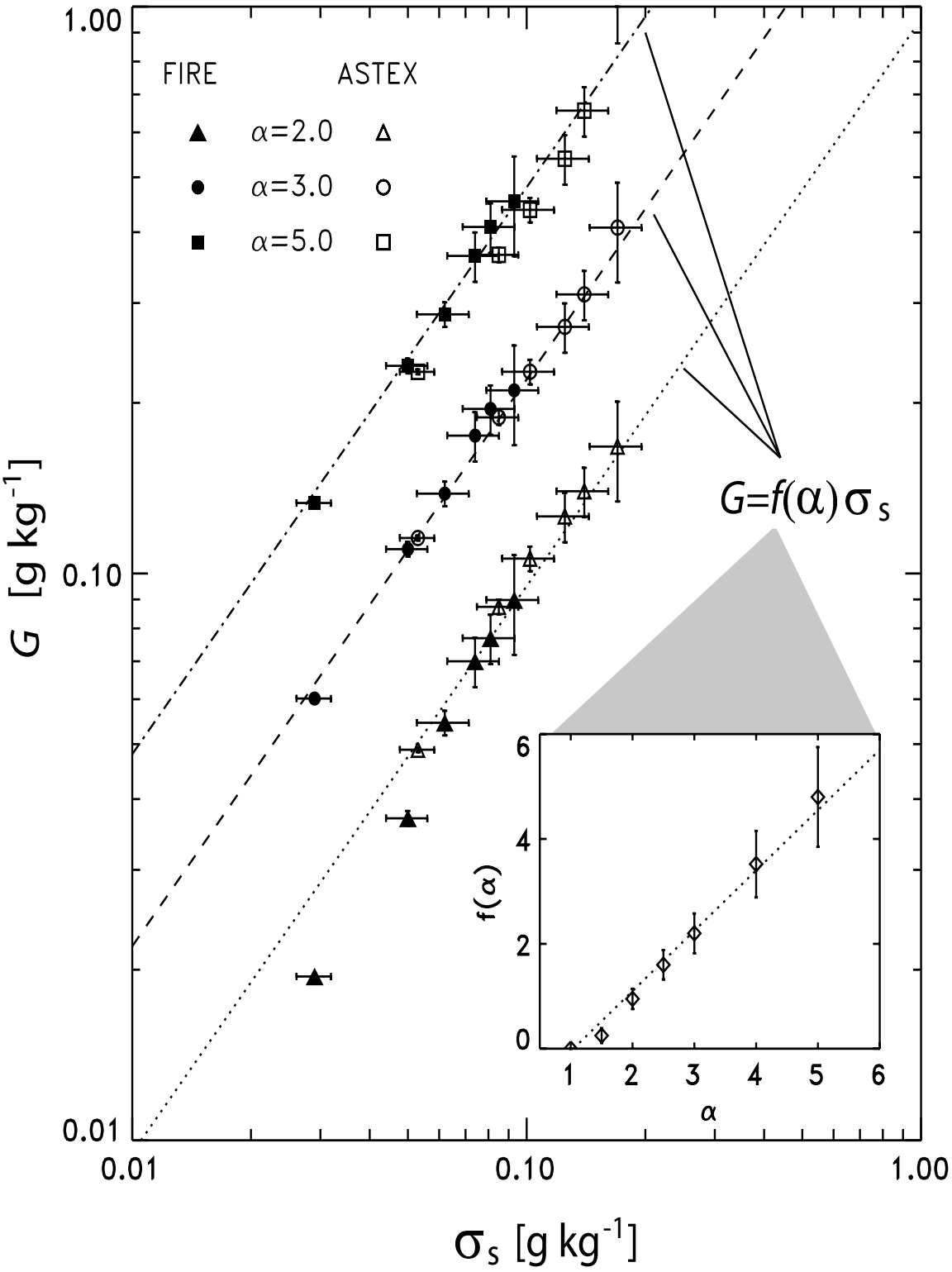
FIRE
ASTEX
α=2.0
α=3.0
α=5.0
G=f(α)σs
f(α)
α
G [g kg-1]
σs [g kg-1]
1.00
0.10
0.01
0.01
0.10
1.00
0
2
4
6
1
2
3
4
5
6

Figure 5:

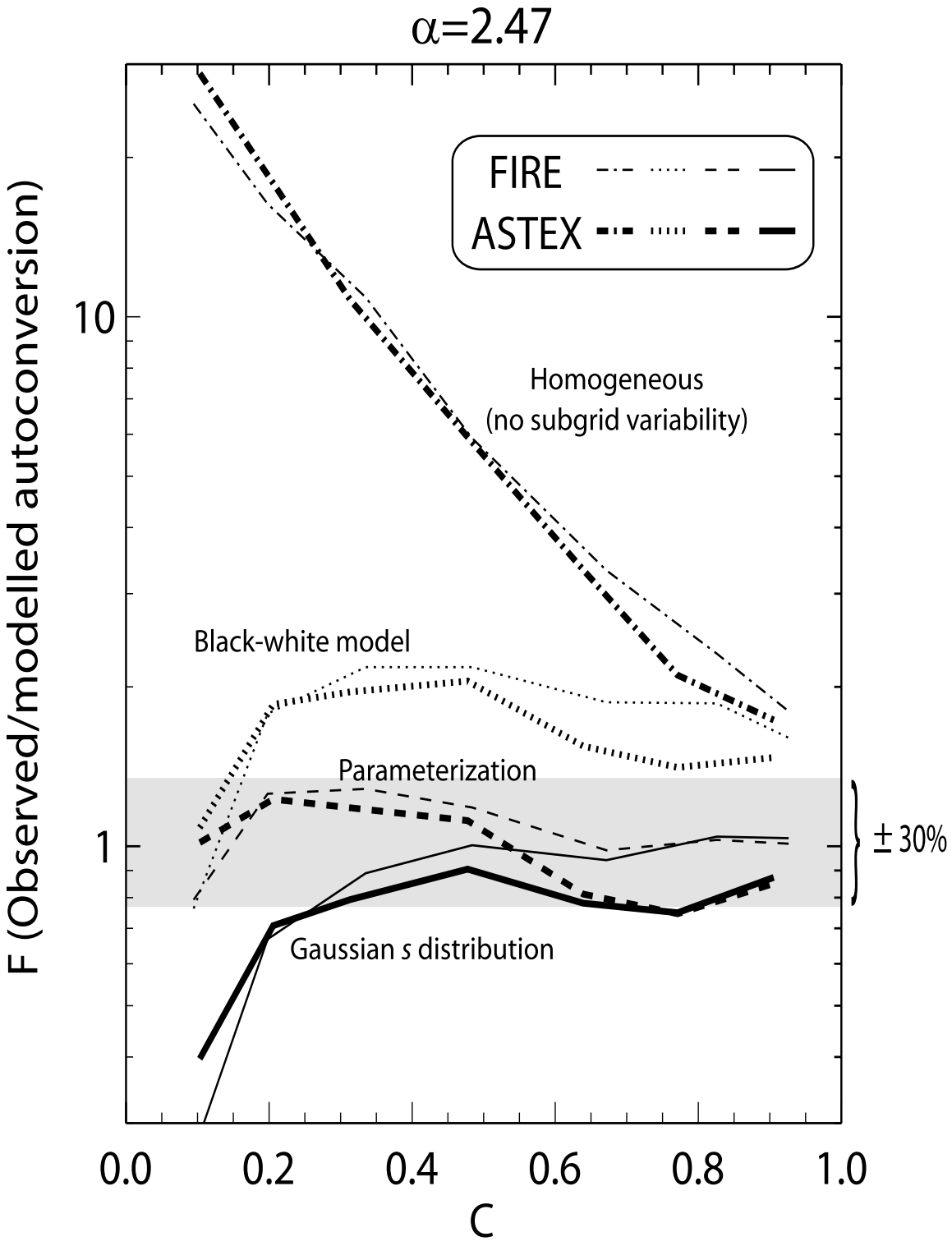
α=2.47
FIRE
ASTEX
Homogeneous
(no subgrid variability)
Black-white model
Parameterization
Gaussian s distribution
± 30%
F (Observed/modelled autoconversion)
10
1
0.0
0.2
0.4
0.6
0.8
1.0
C

Figure 6:

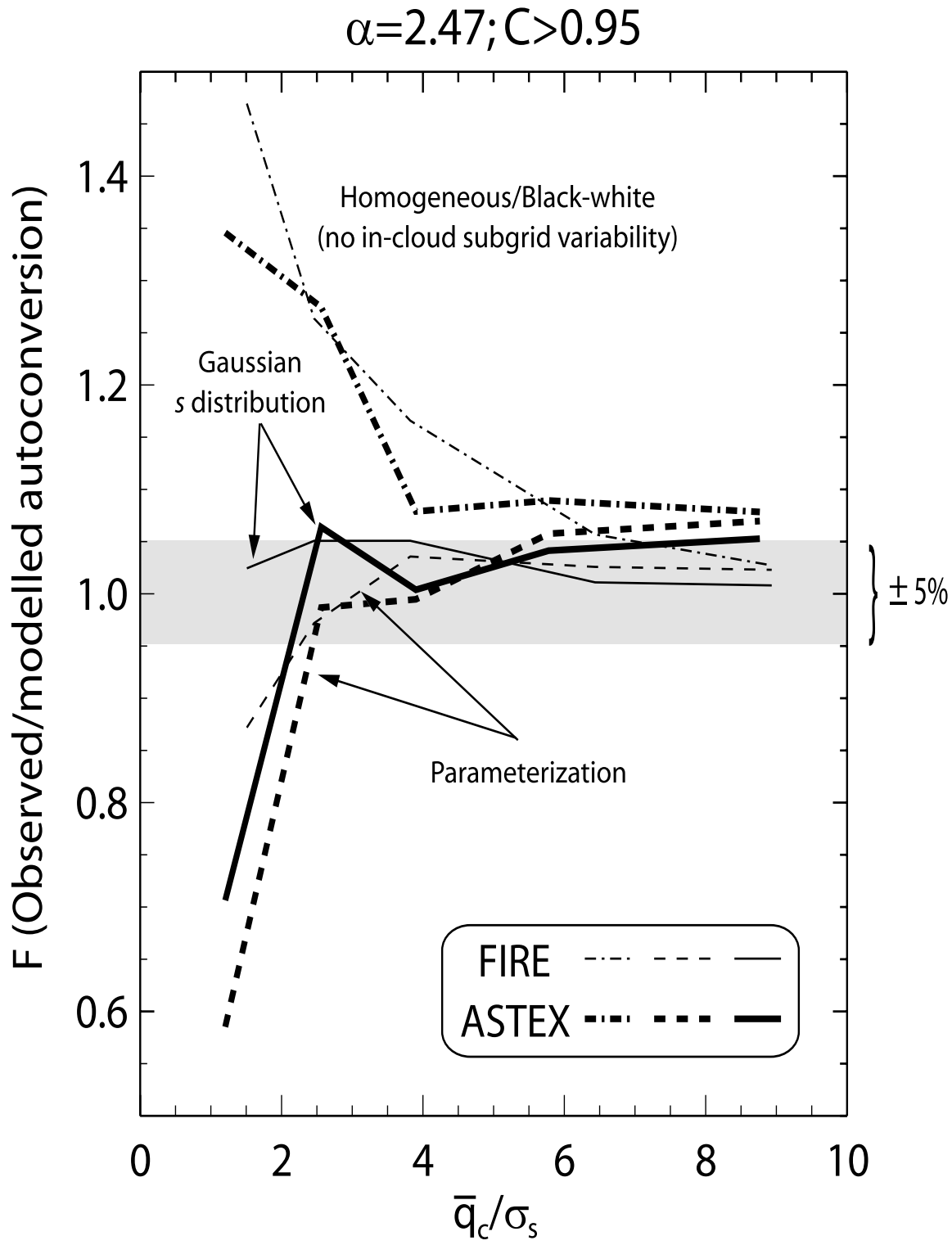
α=2.47; C>0.95
F (Observed/modelled autoconversion)
1.4
1.2
1.0
0.8
0.6
Homogeneous/Black-white
(no in-cloud subgrid variability)
Gaussian
s distribution
Parameterization
± 5%
FIRE
ASTEX
0
2
4
6
8
10
$\bar{q}_c/\sigma_s$

Figure 7: